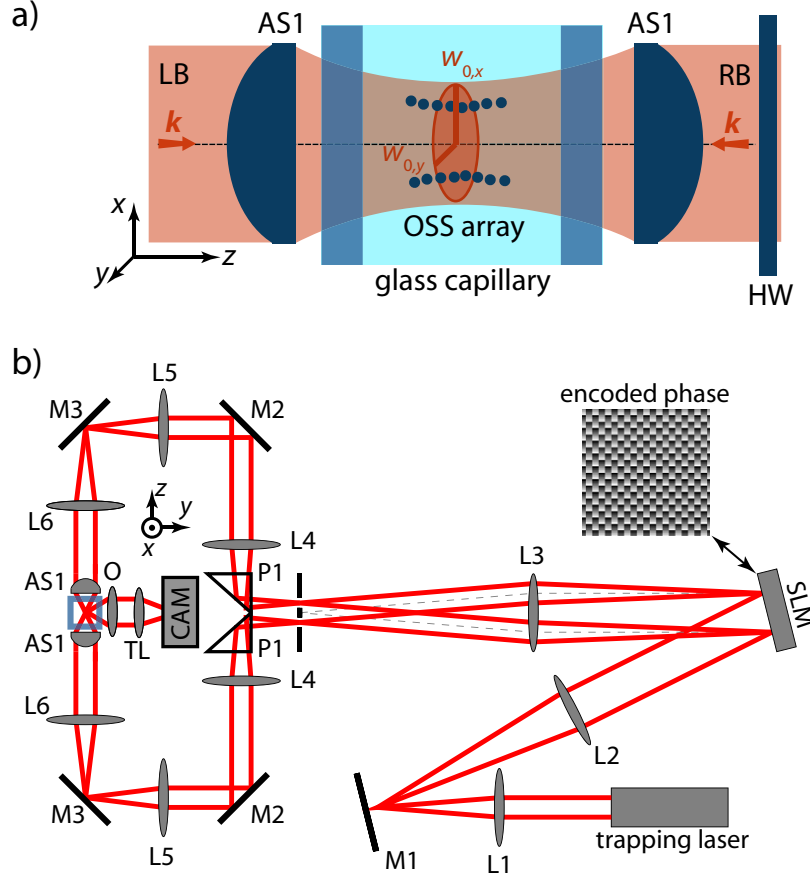


# Dynamic formation of arrays of interacting optical spatial solitons under light-sheet illumination: supplemental document

## 1. EXPERIMENTAL SETUP AND SAMPLE PREPARATION

In the reported experiments, we used a dual-beam optical trap formed by two counter-propagating (C-P) light-sheet beams with linear polarization (wavelength 1064 nm, laser light source ILM-10-1070-LP; IPG Photonics) overlapping inside a vertically oriented glass capillary with square cross-section (inner dimensions  $100 \times 100 \mu\text{m}$ ; Vitrocell) that served as a sample chamber. Resulting quasi-planar colloidal OSS arrays that self-assembled in the trapping region were observed by an optical microscope formed by a long-distance objective (M Plan Apo SL 80X; Mitutoyo), tube lens (focal length 200 mm), and a CMOS camera (acA2000-50gc; Basler) from a direction perpendicular to the plane of the light sheet, see Fig S1a. The trapping beams were transformed using Thorlabs achromatic doublets with anti-reflection coating (ACN254-XXX-C; L1 – L6), dielectric mirrors (PF10-03; M1 – M3), and aspheric lenses with anti-reflection coating (C240TME-C; AS1), see Fig S1b. A collimated Gaussian beam from the laser was first expanded  $2\times$  by a telescope formed by lenses L1 ( $f_1 = 150$  mm) and L2 ( $f_2 = 300$  mm) and subsequently projected on a spatial light modulator (SLM, LCOS X10468-07; Hamamatsu) that served for dynamic shaping of the transverse intensity profiles of the trapping beams. In particular, we created light-sheet beams with transverse beam-waist radii of  $w_{0,x} = 10.5 \mu\text{m}$  and  $w_{0,y} = 1.6 \mu\text{m}$  (values at the trapping location inside the sample chamber) by adjusting the profile of the phase diffraction grating imposed upon the SLM. The phase mask encoded at the SLM diffracted the incident beam into the  $\pm 1^{\text{st}}$  diffraction orders that were used to generate the two C-P trapping beams; the zeroth and higher orders were then blocked by a stop placed in the focal plane of lens L3 ( $f_3 = 400$  mm). The two transmitted  $\pm 1^{\text{st}}$  – order beams were reflected from prisms P1 and collimated by lenses L4 ( $f_4 = 200$  mm). These lenses formed telescopes with the lens L3, projecting the SLM plane on the mirrors M2. Telescopes consisting of lenses L5 ( $f_5 = 100$  mm) and L6 ( $f_6 = 150$  mm) then imaged the SLM plane onto the back focal planes of aspheric lenses AS1 ( $f = 8$  mm, maximal NA = 0.5) that focused the two C-P light-sheet beams into the sample chamber. The focal planes of the two beams created in the trapping region by aspheric lenses AS1 were slightly displaced from each other along the beam propagation direction  $z$  (by approximately  $5 \mu\text{m}$ ) to increase the axial trapping stability [1]. In order to control the relative orientation of the linear polarization of the two trapping beams (parallel vs. perpendicular), a half-wave plate was placed before the back-focal plane of the right aspheric lens AS1.

Polystyrene microspheres with diameters ranging between 60 – 995 nm were dispersed in distilled water and sonicated for several minutes in an ultrasonic bath to disintegrate potential particle clusters. Subsequently, diluted colloidal suspensions were loaded into the capillary sample chamber using a syringe connected to the capillary via flexible tubing. The experiments were started once the pressures at the open end of the capillary and at the sample inlet equilibrated. During the experiments, the syringe remained connected to the sample chamber to eliminate gravity-induced flow along the axis of the capillary ( $x$ -direction).



**Fig. S1.** a) Dual-beam optical trap formed by two linearly polarized, counter-propagating light-sheet laser beams (LB and RB) with orthogonal or parallel polarization controlled by a half-wave plate (HW). Optically trapped and bound particles that form an OSS array located in the plane of the light sheet (the  $xz$ -plane) are observed using a microscope oriented along the  $y$ -axis. b) Experimental setup for the creation and characterization of 2D arrays of interacting OSSs (see the main text for details). AS1: aspheric trapping lenses; CAM: camera; L1 – L6: lenses; M1 – M3: mirrors; O: microscope objective; P1: prisms; SLM: spatial light modulator; TL: tube lens.

## 2. 3D STOCHASTIC SIMULATIONS OF FORMATION OF OSS ARRAYS

To simulate the three-dimensional (3D) stochastic motion of  $N$  optically confined and bound particles forming an OSS array in a viscous fluid, we used Monte-Carlo numerical integration of the overdamped Langevin equation. Using a column vector  $\mathbf{R}$  that combines all  $3N$  coordinates of the particles forming the structure as  $\mathbf{R} = \{x_1, y_1, z_1, \dots, x_N, y_N, z_N\}^T$ , the Langevin equation of motion can be written as

$$\mathbf{\Gamma} \cdot \dot{\mathbf{R}} = \mathbf{F}^{\text{opt}}(\mathbf{R}) + \mathbf{f}(\mathbf{R}, t). \quad (\text{S1})$$

In (S1),  $\mathbf{F}^{\text{opt}}(\mathbf{R})$  is the deterministic optical force and  $\mathbf{f}(\mathbf{R}, t)$  is the stochastic thermal force acting on the system of  $N$  optically trapped and bound particles. Both forces are represented by column vectors with  $3N$  components that combine the Cartesian force components of all  $N$  particles. The  $3N \times 3N$  grand-resistance matrix  $\mathbf{\Gamma}$  then accounts for the hydrodynamic interaction between the particles that are assumed to be spherical [2, 3]. The stochastic force  $\mathbf{f}(\mathbf{R}, t)$  is characterized by zero mean and variance

given by  $\langle \mathbf{f}(\mathbf{R}, t) \otimes \mathbf{f}(\mathbf{R}, t') \rangle = 2k_B T \Gamma \delta(t - t')$ , where  $\otimes$  denotes the outer (dyadic) product and  $\langle \rangle$  represents ensemble averaging. In the numerical implementation, the inverse of the grand-resistance matrix — the grand-mobility matrix  $\mathbf{M} = (\Gamma)^{-1}$  — was used to update the particle positions in a single time step. To calculate  $(\Gamma)^{-1}$ , the third-order approximation of Rotne–Prager–Yamakawa was used, with extra three-particle-interaction refinement for the same-sphere terms [2, 3]. The only deterministic contribution to Eq. (S1) is the optical force  $\mathbf{F}^{\text{opt}}(\mathbf{R})$  evaluated from the Minkowski form of the Maxwell stress tensor [4]. The latter was constructed from the Mie scattering theory for multiple spheres [5] used to solve the electromagnetic interaction of the incident beams and the particles. The localized approximation for a paraxial Gaussian beam [6] was used to model the dual-beam optical trap.

For the integration of Eq. (S1), a simple first-order method was used, with the fixed time step carefully tuned to limit the particle displacements to a fraction of a wavelength in every iteration. For each particular  $N$ , the starting positions of all particles were set to the equilibrium positions of the shorter  $(N - 1)$ -chain, with the extra particle added at one end. For lower values of  $N < 10$ , turning off the stochastic force term  $\mathbf{f}$  helped to accelerate the initial relaxation of the structure along the  $z$ -axis. For this initial part of the simulation, we utilized the MATLAB implementation of a variable-order method for stiff systems `ode15s`. Subsequently,  $\mathbf{f}$  was switched on, and the full 3D stochastic motion of all spheres was simulated. In this simulation phase, the spheres were released from a local stable configuration that was further relaxed or switched into a different stable configuration, thus revealing more realistic correlated dynamics.

The trajectories of individual particles obtained from the stochastic simulations described above were analyzed to determine the effective stiffness of particle confinement in the OSS structure. In the considered quasi-planar trapping geometry based on C-P light-sheet beams (see Fig S1a), the out-of-plane motion of the particles along the  $y$  axis is strongly restricted. Therefore, it is sufficient to carry out the stiffness analysis in the  $xz$ -plane of the light sheet where the spatial confinement due to optical forces is the weakest. The 2D optical potential created in the  $xz$ -plane in the vicinity of the primary OSS chain is approximately harmonic for small displacements of optically trapped and bound particles from their equilibrium configuration. Consequently, it can be characterized by the principal stiffness values along the  $x$  and  $z$  axes. Because the trap stiffness  $\kappa_x$  along the lateral direction  $x$  quantitatively characterizes the strength of interaction between the parallel chains in the OSS structure, we chose  $\kappa_x$  evaluated at the tentative stable positions in the 2D optical potential landscape as the primary indicator of the stability of forming 2D OSS arrays.

### 3. EFFECT OF PARTICLE SIZE ON THE FORMATION AND SPATIAL CONFIGURATION OF 2D OSS ARRAYS

The formation of 2D OSS arrays is a nonlinear process mediated by optical binding forces that are associated with multiple light scattering from the constituent particles. For particles with dimensions comparable to the wavelength of the incident light, the intensity and spatial distribution of the scattered light depend on the particle size in a non-monotonic fashion [7]. Consequently, the landscapes of optical binding forces created in the interference pattern between the incident and scattered light can greatly vary when the particle size changes, particularly in the vicinity of the resonant scattering conditions [8].

To illustrate the strong dependence of the configuration of newly formed 2D OSS arrays on the size of the constituent particles, we simulated the formation of 2D OSS arrays from monodisperse particles whose diameters differ by only 50 nm, keeping the other relevant system parameters (refractive indices of the particles and the ambient medium, spatial profile and intensity of the incident light-sheet beams) constant. For each particle diameter considered (607, 657 and 707 nm), we first determined the stable

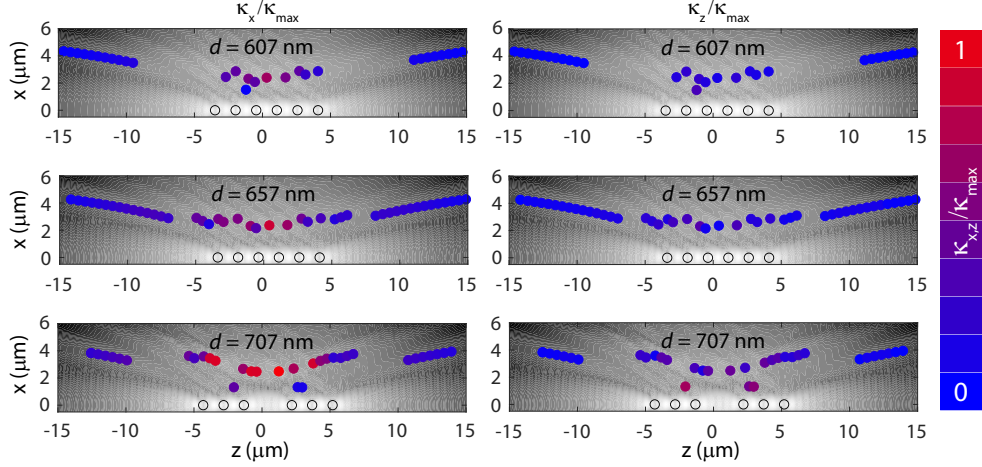


**Fig. S2.** Simulations of the formation of 2D OSS arrays from monodisperse particles of different diameters  $d$  indicated in individual figure panels. The grayscale backgrounds visualize the simulated spatial profiles of the net optical intensity around the primary on-axis OSSs (empty circles), colored circles indicate possible secondary off-axis trapping locations whose normalized lateral stiffness  $\kappa_x / \kappa_{\max}$  (left column) and axial stiffness  $\kappa_z / \kappa_{\max}$  (right column) are color-encoded ( $\kappa_{\max} = \max \{\kappa_x, \kappa_z\}$  for all considered values of  $d$ ). Fixed simulation parameters: particle refractive index 1.59, ambient refractive index 1.33, beam waist radii of the light-sheet beams  $w_{0,x} = 10.5 \mu\text{m}$  and  $w_{0,y} = 1.6 \mu\text{m}$ .

equilibrium configuration of the primary on-axis OSS chain comprising 6 particles. Subsequently, we moved a single probe particle of the same size along a regular 2D grid surrounding the primary OSS and determined the value of  $\mathbf{F}^{\text{opt}}(x, z)$  exerted on the probe particle at the given location  $[x, z]$ . Finally, we calculated the values of the trap stiffness  $\kappa_x, \kappa_z$  that quantitatively characterize the components of  $\mathbf{F}^{\text{opt}}(x, z)$  along the  $x$  and  $z$  axes in the vicinity of the tentative stable positions in the 2D optical potential landscape (see Section 2 for details).

Figure S2 summarizes the results of these simulations. The grayscale backgrounds in individual panels visualize the spatial profiles of the intensity of the net optical field formed in the vicinity of the primary OSS chains (empty circles). The colored circles then mark possible off-axis trapping locations created in the net optical field around the primary OSS, with the color encoding the magnitude of the normalized lateral trap stiffness  $\kappa_x / \kappa_{\max}$  and axial trap stiffness  $\kappa_z / \kappa_{\max}$  (red color: maximal normalized stiffness, blue color: minimal normalized stiffness,  $\kappa_{\max} = \max \{\kappa_x, \kappa_z\}$  for all considered particle sizes). The stability of confinement in these secondary optical traps is determined by the modulation depth of the off-axis optical intensity. In general, off-axis traps with higher values of  $\kappa_x, \kappa_z$  are more likely to function as stable nucleation sites for secondary OSS chains. The comparison of the results obtained for different particle sizes clearly indicates that the configuration of the primary OSS chain and the locations and stability of the possible nucleation sites for the secondary chains vary largely with the particle size. Similar changes of OSS configuration can then be induced by varying the refractive indices of the particle / ambient medium or the intensity profiles of light-sheet beams.

It is worth noting that the variations in the overall configuration of 2D OSS arrays observed with changing particle size result from the complex force interactions in the physical system “particles + interference light field”; they are not artifacts introduced by numerical errors or approximations adopted in the simulation procedure.

#### 4. CHARACTERIZATION OF OPTICAL FORCES WITHIN OSS ARRAYS USING EXPERIMENTALLY RECORDED TRAJECTORIES

As stated in Section 2, a collection of  $N$  colloidal particles optically trapped and bound in a viscous liquid represents an overdamped dynamical system the trajectory of which evolves according to the  $3N$ -dimensional Langevin equation of motion (S1) with coupled degrees of freedom  $\mathbf{R} = \{x_1, y_1, z_1, \dots, x_N, y_N, z_N\}^T$ . The actual experimental trajectory  $\mathbf{R}(t)$  of the system, together with (S1), can in turn be used to infer the spatial profile  $\mathbf{F}^{\text{opt}}(\mathbf{R}) = \{F_{x,1}^{\text{opt}}(\mathbf{R}); F_{y,1}^{\text{opt}}(\mathbf{R}); F_{z,1}^{\text{opt}}(\mathbf{R}); \dots, F_{x,N}^{\text{opt}}(\mathbf{R}); F_{y,N}^{\text{opt}}(\mathbf{R}); F_{z,N}^{\text{opt}}(\mathbf{R})\}$  of the net optical force field acting on the system.

As discussed in [9], Bayesian inference is a powerful approach for the quantitative characterization of optical force fields that uses a maximal-likelihood approach for extracting the parameters of interest solely from the discrete trajectories of the system of optically trapped and bound particles recorded in the presence of detection noise. Briefly, the desired characteristics of the optical force field are identified as the values that maximize the conditional probability distributions of the actual recorded trajectories, parametrized using the appropriate form of the Langevin equation of motion (S1) for the particular studied system. In this sense, the particle trajectories serve as probes of the local force field, as stated in the main article.

#### REFERENCES

1. S. A. Tatarkova, A. E. Carruthers, and K. Dholakia, “One-Dimensional Optically Bound Arrays of Microscopic Particles,” *Phys. Rev. Lett.* **89**, 283901 (2002).
2. P. Reuland, B. U. Felderhof, and R. B. Jones, “Hydrodynamic interaction of two spherically symmetric polymers,” *Phys. A Stat. Mech. its Appl.* **93**, 465–475 (1978).
3. B. Carrasco and J. G. de la Torre, “Improved hydrodynamic interaction in macromolecular bead models,” *J. Chem. Phys.* **111**, 4817–4826 (1999).
4. O. Farsund and B. U. Felderhof, “Force, torque, and absorbed energy for a body of arbitrary shape and constitution in an electromagnetic radiation field,” *Phys. A* **227**, 108–130 (1996).
5. D. Mackowski, “The Extension of Mie Theory to Multiple Spheres,” in *Mie Theory Basics Appl.*, W. Hergert and T. Wriedt, eds. (Springer Berlin Heidelberg, Berlin, Heidelberg, 2012), pp. 223–256.
6. G. Gouesbet, J. Lock, and G. Grehan, “Generalized Lorenz-Mie theories and description of electromagnetic arbitrary shaped beams: Localized approximations and localized beam models, a review,” *J. Quant. Spectrosc. Radiat. Transf.* **112**, 1–27 (2011).
7. M. Kerker, *The Scattering of Light and Other Electromagnetic Radiation*. (Academic Press, New York, 1969).
8. P. Zemánek, A. Jonáš, and M. Liška, “Simplified description of optical forces acting on a nanoparticle in the Gaussian standing wave,” *J. Opt. Soc. Am. A* **19**, 1025–1034 (2002).
9. M. Šiler, V. Svak, A. Jonáš, S. Simpson, O. Brzobohatý, and P. Zemánek, “Bayesian estimation of experimental parameters in stochastic inertial systems: theory, simulations, and experiments with objects levitated in vacuum,” *Phys. Rev. Appl.* **19**, 064059 (2023).